High-temperature sensor using a Fabry-Perot interferometer based on solid-core photonic crystal fiber

Jing Zhang (张 菁), Hao Sun (孙 浩), Qiangzhou Rong (荣强周), Yue Ma (马 玥), Lei Liang (梁 磊), Qinfang Xu (徐琴芳), Pei Zhao (赵 佩), Zhongyao Feng (冯忠耀), Manli Hu (忽满利), and Xueguang Qiao (乔学光)*

Department of Physics, Northwest University, Xi'an 710069, China

**Corresponding author: xgqiao@nwu.edu.cn*

Received November 2, 2011; accepted February 13, 2012; posted online April 12, 2012

A micro Fabry-Perot interferometer (M-FPI) is constructed by splicing a short section of polarization-maintaining photonic crystal fiber (PM-PCF) to an end-cleaved single-mode fiber with controllable offset. Due to the high effective optical path difference induced by the solid core of the PCF, the M-FPI has an ultrasmall cavity of approximately 110 μm. The temperature sensitivity within a range from 33 °C to approximately 600 °C is measured to be 13.8 pm/°C, which shows good agreement with the theoretical result. This proposed sensor has the advantages of ultracompact size and high stability. Therefore, it is suitable for various space-limited sensing applications in harsh environments.

OCIS codes: 060.0060, 060.2310, 060.2370, 060.2430.
doi: 10.3788/COL201210.070607.

In-fiber interferometer sensors exhibit the outstanding advantages over conventional fiber sensors, such as light weight, flexibility, good electromagnetic interference immunity, etc. These advantages make them good candidates for sensing applications in space-limited harsh environments, especially for high-temperature measurement[1]. In past decades, various approaches have been developed to fabricate in-fiber interferometers, including intermodal interferometers based on different fibers, such as multi-mode fibers (MMFs)[2], hollow-core fibers[3], and in-fiber Mach-Zehnder interferometers (MZIs) based on a MM–SM–MM (MM: multi-mode; SM: single-mode) structure[4] or by adopting a section of twin-core fiber[5]. Generally, temperature sensors based on these methods are able to provide a sensitivity of tens of pm/°C; however, most of these approaches work on transmission. Additionally, a Michelson interferometer formed by using a single-mode fiber (SMF) mated with a short section of dispersion-compensation fiber (DCF) recently achieved a relative high temperature sensitivity of 68 pm/°C[6]. Aside from the methods above, the fiber Fabry-Perot interferometer (FPI) sensors are particularly attractive for high-temperature measurement[7−9]. The physical lengths of these micro air-gap cavities are limited to several millimeters or less, which gives them overwhelming advantages for high-temperature sensing. However, complicated fabrication processes are required to form the air-gap cavity, such as inserting two sapphire fibers into a zirconium tube[7], etching[8], laser micromachining[9], and sandwiching a short section of hollow crystal fiber between two standard SMFs[1]. In contrast, an ultrasmall Fabry-Perot cavity on a taper tip with an extremely small size was proposed by Kou *et al.*[10]. However, the fabrication process is extremely complicated and the taper should be very soft, which would cause a drawback of poor resistibility to vibration and air drift. Recently, Hu *et al.* proposed a miniaturized multiplexed fiber interferometer (MFI) using a hollow fiber with a sphere-ended hollow-core fiber. However, the unsmooth profile of the low-frequency envelope fringe will cause difficulty in measurement and a large error[11].

Recently, Dong *et al.* reported a polarization-maintaining photonic crystal fiber (PM-PCF) based interferometer and demonstrated its sensing capability[12]. Despite its advantages of compact size and easy fabrication, this approach is unsuitable for remote sensing because it works on transmission. In this letter, we fabricated a micro reflectivity interferometer by splicing the end of the SMF-28 fiber to the cleaved end of a tiny particle of PM-PCF with a controllable core offset using a fusion splicer. The fabrication was accomplished using a manually operated commercially fusion splicer (FSM60, Fujikura). The sensing principle analysis and a temperature test with a range of 33−600 °C were carried out. A temperature sensitivity of 13.8 pm/°C was obtained by monitoring the dip wavelength shift, which showed good agreement with the theoretical analysis.

The proposed interferometer is schematically illustrated in Fig. 1. A length of PM-PCF was spliced to a standard SMF with a lateral offset splice (the offset was approximately 5 μm). The PM-PCF had a pure silica core symmetrically with two 7.5-μm air holes at its sides, as the micrograph image shows in Fig. 1. With the offset, a weak mirror was formed by the core-air interfaces at the splice facet, combining with the end facet of the PM-PCF construct the FPI. Owning to the Fresnel reflection, a portion of core modes were reflected at the core-air interface at the facet, whereas the remaining ligths were reflected after traveling through the solid core of the PCF, which consequently induced an optical path difference between the two split modes. As the reflected powers recombined with each other, an interference spectrum was generated. For the proposed interferometer, a relatively large optical path difference can be induced by extremely short PM-PCF, and the length of the PM-PCF is limited to be few hundred micrometers.

Here, we suppose I_1 and I_2 to be the intensities of the

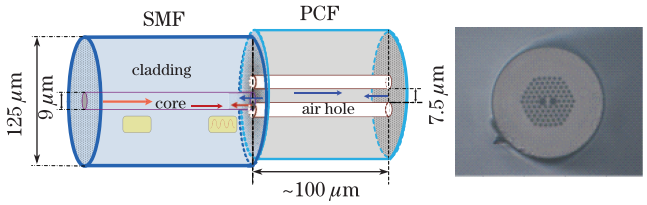

Fig. 1. Diagram of the proposed FPI and the cross-section of the PM-PCF.

two reflected beams. Thus, the intensity of spectral response of the FPI can be expressed as

$$I = I_1 + I_2 + 2\sqrt{I_1 I_2}\cos\varphi, \tag{1}$$

where $\varphi = 4\pi n_{\text{eff}} L/\lambda$ is the phase difference induced by the PM-PCF, n_{eff} is the effective refractive index of pure silica, L is the length of the PM-PCF, and λ is the operation wavelength. Because the phase difference satisfies the interference condition $\varphi = 2m\pi$(m is integer), the corresponding dip wavelengths can be expressed as

$$\lambda_m = \frac{2n_{\text{eff}}L}{m}. \tag{2}$$

From Eq. (2), the free spectral range (FSR) between two interference minima can be approximated as

$$\text{FSR} = \frac{\lambda^2}{2n_{\text{eff}}L}. \tag{3}$$

As Eq. (3) shows, the FSR is related to the effective refractive index and the length of the PM-PCF. Unlike the sensor in Ref. [6], in which the phase difference was induced by the core and cladding of DCF with index difference of approximately 2.1×10^{-2}, the phase shift of our FPI is directly induced by the core of a PM-PCF with an effective index of 1.4575, which is much larger than that in the previous works, thereby contributing to an extraordinarily compact size of hundreds of millimeters.

When the temperature applied to the FPI changes, the effective index n_{eff} and the length L will change accordingly, which subsequently result in two effects: 1) blueshift of the resonance wavelength and 2) variation with temperature of the wavelength spacing. According to Eq. (2), the wavelength shift of the resonance dips can be expressed as

$$\Delta\lambda = \left(\frac{\partial n_{\text{eff}}}{\partial T\cdot n_{\text{eff}}} + \frac{\partial L}{\partial T\cdot L}\right)\Delta T\lambda_{\text{m}} = (\alpha+\varepsilon)\Delta T\lambda_{\text{m}}, \tag{4}$$

where $\alpha = 8.3\times10^{-6}$ °C and $\varepsilon = 0.55\times10^{-6}$ °C are the thermal expansion coefficient and the thermo-optic coefficient of the pure silica, respectively. The temperature sensitivity of the proposed FPI was calculated to be 13.7 pm/ °C at the operation wavelength of 1 550 nm based on Eq. (4).

Figure 2(a) shows the microscope photograph (200×) of the proposed micro FPI (M-FPI) with approximately 100-μm PM-PCF (PM-125-03, YSL Photonics). Figure 2(b) shows the spectral response of the sensor with no coating film on the end facet of PM-PCF, which exhibits a sufficiently high signal-to-noise ratio (SNR) of approximately 10 dB and a relatively low loss of approximately 16 dB, making it easy to observe the dip wavelength shift during the sensing course. For case of the proposed sensor, the theoretical FSR was determined to be 8.24 nm based on Eq. (3), which agreeed well with the result in the experiment. This result also verifies that our method is based on the Fabry-Perot interference, whereas the configuration in Ref. [12] is based on the interference between the core modes and cladding modes in PM-PCF (15-nm FSR by using 11-mm PM-PCF). The corresponding spatial spectrum in Fig. 2(c) shows some higher frequencies, indicating that some weak cladding modes are excited and interfered with other modes. Nevertheless, these frequencies would not cause an obvious effect due to their low intensities and the slight difference between the temperature responses of the cladding modes and the core mode, as verified in Refs. [12,13].

Figure 3 shows the experimental setup. Light generated by a C+L band broad-band source (BBS) was launched into the FPI though port 1 of a circular, and the output light was extracted from port 2 into an optical spectrum analyzer (OSA) with a resolution of 0.02 nm for measurement. To investigate the temperature responsibility, the FPI was placed in a tube furnace with a thermocouple to monitor the temperature. The temperature was gradually raised to 582 °C, and then naturally cooled down to room temperature. To ensure a uniform temperature measured by the sensing FPI and the monitoring thermal-electric coupler, the temperature was kept constant for 15 min before each measurement. Figures 4(a) and (b) show the summarized spectra at different

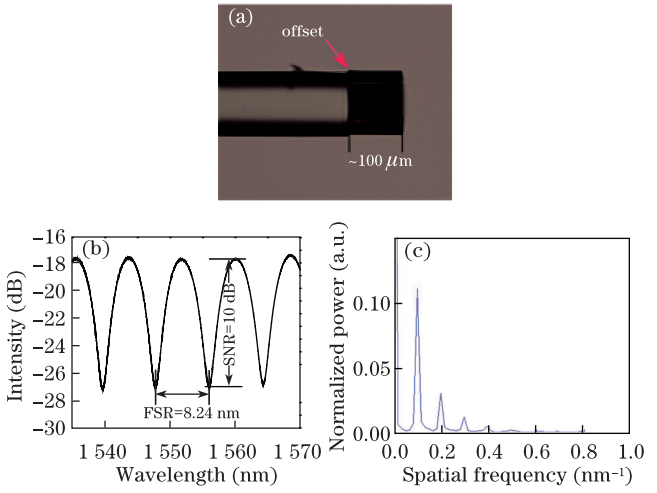

Fig. 2. (a) Microscope image of the sensor with length of ~100 μm; (b) spectral response of the proposed sensor at 33 °C; (c) corresponding spatial spectrum.

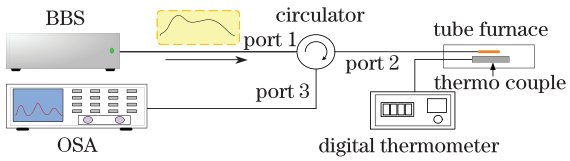

Fig. 3. Experimental setup for the temperature test.

temperatures in the heating and the cooling processes, respectively. Here, we use the position of the dip Ds as the measured parameter, and the wavelength shift with respect to temperature is shown in Fig. 5. The slope of the straight line obtained from data fitting shows the sensitivity of temperature sensing. Thus, the sensitivities of the two processes are determined to be 13.8 and 14.1 pm/°C, respectively, which are in perfect agreement with the theoretical result of 13.7 pm/°C. Meanwhile, R^2 values of the heating and cooling processes are 0.993 and 0.9968, respectively. As Figs. 4(a) and (b) show, the spectral response of the FPI is very stable and no obvious deterioration occurred at high temperature.

In conclusion, we propose and demonstrate a high-temperature sensor based on an ultracompact FPI. The FPI, formed by splicing an end cleaved with approximately 100-μm PM-PCF to SMF, is able to provide an extinction ratio of approximately 10 dB and FSR of 8.24 nm. In our temperature test, the surrounding temperature vibration is monitored by detecting the wavelength shift of the interferometer dip induced by the thermal effects of the PCF using OSA. Experimental results exhibited sensitivity of 13.8 pm/°C within a measurement range from 33 to 600 °C, which is in perfect agreement with the theoretical results. The proposed M-FPI is ultracompact in size, simple to fabricate, and cost-effective. More importantly, the ultrasmall mass enables rapid reaction ability to temperature changes. These advantages make it suitable for application in high temperature with limited space in harsh environments.

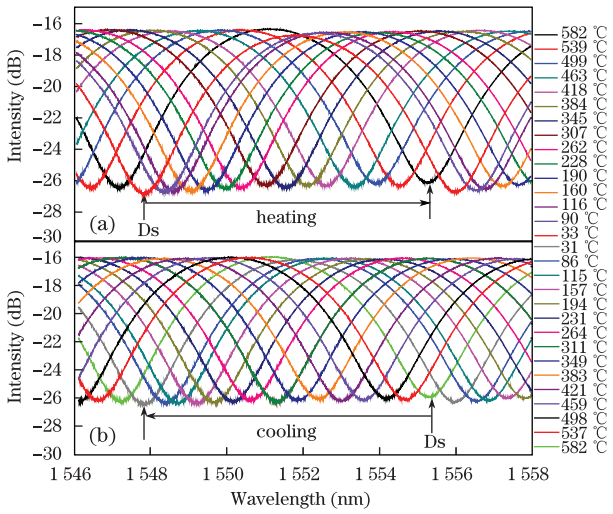

Fig. 4. Transmission spectra of the proposed sensor in (a) heating and (b) cooling processes.

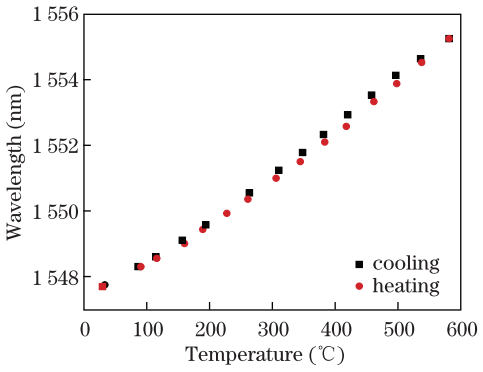

Fig. 5. Wavelength shift of the dip Ds under different temperatures.

This work was supported by the National Natural Science Foundation of China (Nos. 61077006, 60727004, and 61077060), the National "863" Program of China (Nos. 2007AA03Z413 and 2009AA06Z203), the Ministry of Education Project of Science and Technology Innovation (No. Z08119), the Ministry of Science and Technology Project of International Cooperation (No. 2008CR1063), Shaanxi Province Project of Science and Technology Innovation (Nos. 2009ZKC01-19 and 2008ZDGC-14), and Northwestern University Teaching and Research Project (Nos. YC07059 and KJG10036).

References

1. Y. J. Rao, T. Zhu, X. C. Yang, and D. W. Duan, Opt. Lett. **32,** 18 (2007).
2. E. B. Li, X. L. Wang, and C. Zhang, Appl. Phys. Lett. **89,** 091119 (2006).
3. B. Dong and E. J. Z. Hao, Appl. Opt. **50,** 18 (2011).
4. L. V. Ng uyen, D. S. Hwang, S. Moon, D. S. Moon, and Y. J. Chung, Opt. Express **16,** 11369 (2008).
5. R. Zhao, L. Pei, Z. Li, T. Ning, L. Fan, and W. Jiang, Chin. Opt. Lett. **9,** 062801 (2011).
6. B. Dong, L. Wei, and D. P. Zhou, Appl. Opt. **48,** 33 (2009).
7. J. J. Wang, B. Dong, E. Lally, J. M. Gong, M. Han, and A. B. Wang, Opt. Lett. **35,** 619 (2010).
8. T. Zhao, Y. Gong, Y. Rao, Y. Wu, Z. Ran, and H. Wu, Chin. Opt. Lett. **9,** 050602 (2011).
9. Y. J. Rao, M. Deng, D. W. Duan, X. C. Yang, T. Zhu, and G. H. Cheng, Opt. Express **15,** 14123 (2007).
10. J. L. Kou, J. Feng, L. Ye, F. Xu, and Y. Q. Lu, Opt. Express **18,** 14245 (2010).
11. D. J. J. Hu, Y. Wang, J. L. Lim, T. Zhang, K. Mileńko, Z. Chen, M. Jiang, G. Wang, F. Luan, P. P. Shum, Q. Sun, H. Wei, W. Tong, and T. R. Wolińkietc, IEEE Sensor. J. **99,** 1-1 (2011).
12. B. Dong, D. P. Zhou, and L. Wei, J. Lightwave Technol. **28,** 1011 (2010).
13. X. W. Shu, K. Sugden, and I. Bennion, Meas. Sci. Technol. **21,** 094003 (2010).